# Computation of Molecular Electrostatics with Boundary Element Methods

Jie Liang* and Shankar Subramaniam*#
*National Center for Supercomputing Applications and #Beckman Institute, Department of Molecular and Integrative Physiology, Center for Biophysics and Computational Biology, University of Illinois at Urbana-Champaign, Urbana, Illinois 61801 USA

ABSTRACT In continuum approaches to molecular electrostatics, the boundary element method (BEM) can provide accurate solutions to the Poisson-Boltzmann equation. However, the numerical aspects of this method pose significant problems. We describe our approach, applying an alpha shape-based method to generate a high-quality mesh, which represents the shape and topology of the molecule precisely. We also describe an analytical method for mapping points from the planar mesh to their exact locations on the surface of the molecule. We demonstrate that derivative boundary integral formulation has numerical advantages over the nonderivative formulation: the well-conditioned influence matrix can be maintained without deterioration of the condition number when the number of the mesh elements scales up. Singular integrand kernels are characteristics of the BEM. Their accurate integration is an important issue. We describe variable transformations that allow accurate numerical integration. The latter is the only plausible integral evaluation method when using curve-shaped boundary elements.

## INTRODUCTION

Electrostatic interactions play an important role in macromolecular structure and function. The continuum approach provides a convenient route for understanding molecular electrostatic interactions (Gilson et al., 1985; Allison et al., 1986; Rashin et al., 1986; Sharp and Honig, 1990; Madura et al., 1994). Here the molecule is modeled as a cavity of low interior dielectric constant embedded in a continuous medium of solvent of high dielectric constant. The interior of the cavity contains point charges representing charge distributions on atoms in the molecule. The Poisson equation or Poisson-Boltzmann equation is then solved for the electrostatic potentials over the space. Two widely used methods for solving the continuum electrostatic problems are the finite-difference method (FDM) and the boundary element method (BEM). FDM employs a box of three-dimensional cubic grids, where the solute molecule and a portion of surrounding continuum solvent are contained. The electrostatic potentials are then directly solved from the partial differential equation on the grid points (Warwicker and Watson, 1982; Gilson et al., 1985; Davis and McCammon, 1990; Sharp and Honig, 1990; Madura et al., 1994). BEM uses Green's second identity to transform the elliptic partial differential equation over a molecule-containing volume to integral equations over the surface of the molecule (Zauhar and Morgan, 1985, 1988, 1990; Yoon and Lenhoff, 1990; Juffer et al., 1991; Zhou, 1993a; Bharadwaj et al., 1995; Zauhar and Varnek, 1996). With a discretized surface description, the integral equations are then solved numerically. BEM can also be thought of as computing a distribution of the induced point charges (single layer) due to the polarization of the solvent and a distribution of the induced point dipoles (double layer) due to the effects of the ions present in the solvent.

The boundary element method can treat both the molecular shape and the interior charges very accurately. It discretizes the surface of the molecule and relies only on the surface integrals of the molecule. The collection of the discrete surface elements makes it possible to represent the shape of the molecule precisely. This is in contrast to the nature of the molecular boundary imposed by cubic volume elements in a finite-difference method. The interior charges can also be placed at their exact locations, because these charges no longer need to coincide with grid points. Therefore, no distortion in molecular charge distribution is introduced, unlike in FDM, where artificial distribution of fractional charges onto neighboring grid points is used. As a result, BEM has no need for special remedies such as focusing and rotational averaging, which are commonly practiced in finite-difference methods. The self energy artifacts (Bruccoleri, 1993) in the calculation of reaction potential also do not exist in BEM. In addition, the space outside the molecule does not have to be discretized in BEM, and therefore the potential at places distant from the molecule can be computed accurately. Furthermore, because there is no finite-volume box involved, there are no artificial boundary conditions akin to those imposed in the finite-difference method when systems infinite relative to molecular dimensions are modeled (i.e., in many cases the boundary faces of the box are within distances to the molecule edge that are comparable to the molecular size).

In this paper, we apply accurate methods to compute molecular shapes for use in BEM electrostatics calculations. We also determine the desired formulation of BEM, which has the advantage of numerical stability. We show that such

*Received for publication 30 December 1996 and in final form 25 June 1997.*

Address reprint requests to Dr. Shankar Subramaniam, Beckman Institute, Department of Molecular and Integrative Physiology, Center for Biphysics and Computational Biology, University of Illinois at Urbana-Champaign, Urbana, IL 61801. Tel.: 217-244-4489; Fax: 217-244-2909; E-mail: shankar@uiuc.edu.



0006-3495/97/10/1830/12 $2.00

numerical stability is scalable when more mesh elements are introduced under this formulation and provides an important advantage for practical computation. Through an example, we demonstrate that this characteristic is not shared by the other widely used BEM formulations for molecular electrostatics. We further report the development of effective methods for numerical integration of singular and near-singular integrands, which are essential for accurate BEM calculation.

## POISSON-BOLTZMANN EQUATION AND THE FORMULATION OF THE INTEGRAL EQUATIONS

For a molecule $\Omega$ embedded in an ionic solution, its interior (int $\Omega$) and the exterior ($\mathbb{R}^3 - \Omega$) are separated by the surface of the molecule, i.e., the boundary $\partial\Omega$ of the molecule. For any three-dimensional point $x \in \mathbb{R}^3$ in the interior of the molecule, the electrostatic potential $u^i(x)$ is governed by the Poisson equation

$$\nabla^2 u^i(x) = -\frac{1}{\epsilon_i} \sum_{k=1}^{n} q_k \cdot \delta(x - x_k), \quad \text{for } x \in \text{int } \Omega \tag{1}$$

Here $\epsilon_i$ is the uniform dielectric constant inside a molecule, $\delta(x)$ is the three-dimensional delta function, and the interior of the molecule contains $n$ point charges $q_k$ at position $x_k$. For any point in the exterior $x \in \mathbb{R}^3 - \Omega$, the potential $u^e(x)$ is governed by the linearized Poisson-Boltzmann equation

$$\nabla^2 u^e(x) = \kappa^2 \cdot u^e(x), \quad \text{for } x \in \mathbb{R}^3 - \Omega \tag{2}$$

Here $1/\kappa$ is the Debye length characterizing the screening effect due to the presence of the ions in the solvent. On the surface of the molecule $\partial\Omega$, we denote the normal derivative of the potential at $x$ along the outward unit normal vector $n_x$ at $x$ as $g$ (i.e., $g^i(x) = \partial u^i(x)/\partial n_i$ and $g^e(x) = \partial u^e(x)/\partial n_x$); then we have the interface condition

$$u^i(x) = u^e(x) \quad \text{and} \quad g(x) \equiv g^i(x) = \frac{\epsilon_e}{\epsilon_i} \cdot g^e(x) \tag{3}$$

The above equations can be formulated into integral equations by a standard BEM technique (Brebbia et al., 1984). Two different formulations have been reported; details are described by Yoon and Lenhoff (1990) and Juffer et al. (1991). We call them the nonderivative method (nBEM) (Zauhar and Morgan, 1990; Yoon and Lenhoff, 1990; Zhou, 1993b) and the derivative method (dBEM) (Juffer et al., 1991). In this section we briefly outline the main steps in the formulations and summarize the resulting equations and formulae.

### nBEM formulation

Applying Green's second identity,

$$\int_V (\phi \nabla^2 \psi - \psi \nabla^2 \phi) \cdot dV = \int_S (\phi \nabla \psi - \psi \nabla \phi) \cdot dS \tag{4}$$

to the Poisson Eq. 1, we can obtain the integral equation for potential in the interior:

$$\omega(x) \cdot u^i(x) = \int_{\partial\Omega} K_1(x, y) \cdot g(y) \cdot d\sigma_y - \int_{\partial\Omega} K_2(x, y) \cdot u(y) \cdot d\sigma_y + \sum_{k=1}^{n} \frac{q_k}{4\pi\epsilon_i |x - x_k|}, \quad x \in \text{int } \Omega, \quad y \in \partial\Omega \tag{5}$$

Here $x$ is the location of an interior point, $y$ is a surface point, and $\omega(x)$ is the solid angle at point $x$. For interior $x \in$ int $\Omega$, $\omega(x) = 1$ (the full angle is counted as 1). The integration is over all points on the surface of the molecule. $K_i$ are kernel integrands and are explained later.

Similarly, applying Green's second identity to the linearized Poisson-Boltzmann Eq. 2, we obtain the integral equation for the exterior potential:

$$\omega(x) \cdot u^e(x) = -\frac{\epsilon_e}{\epsilon_i} \int_{\partial\Omega} K_3(x, y) \cdot g(y) \cdot d\sigma_y + \int_{\partial\Omega} K_4(x, y) \cdot u(y) \cdot d\sigma_y, \quad x \in \mathbb{R}^3 - \Omega, \quad y \in \partial\Omega \tag{6}$$

Again here $\omega(x) = 1$.

For surface points $x \in \partial\Omega$, the solid angle for the above two equation is no longer the full angle. For example, if point $x$ is in a smooth neighborhood, then $\omega(x) = 1/2$. Combining integral equations 5 and 6 with the interface condition (Eq. 3), we obtain the boundary integral equations for surface potential and its normal derivative:

$$\frac{1}{2} \cdot u(x) - \int_{\partial\Omega} K_1(x, y) \cdot g(y) \cdot d\sigma_y + \int_{\partial\Omega} K_2(x, y) \cdot u(y) \cdot d\sigma_y = \sum_{k=1} \frac{q_k}{4\pi\epsilon_i |x - x_k|} \tag{7}$$

$$\frac{1}{2} \cdot u(x) + \frac{\epsilon_e}{\epsilon_i} \int_{\partial\Omega} K_3(x, y) \cdot g(y) \cdot d\sigma_y - \int_{\partial\Omega} K_4(x, y) \cdot u(y) \cdot d\sigma_y = 0 \tag{8}$$

The integrand kernels in these integral equations are

$$K_1(x,y)=\frac{1}{4\pi|x-y|},\quad K_2(x,y)=\frac{1}{4\pi}\cdot\frac{\partial}{\partial n_y}\left(\frac{1}{|x-y|}\right)$$
$$K_3(x,y)=\frac{e^{-\kappa|x-y|}}{4\pi|x-y|},\quad K_4(x,y)=\frac{1}{4\pi}\cdot\frac{\partial}{\partial n_y}\left(\frac{e^{-\kappa|x-y|}}{|x-y|}\right) \tag{9}$$

where $K_1$ is the free-space Green's function (or the fundamental solution) to the Poisson's equation (Eq. 1), and $K_3$ is the free-space Green's function (or the fundamental solution) to the linearized Poisson-Boltzmann equation (Eq. 2). $K_3$ and $K_4$ are their respective directional derivatives along the outward normal vectors at $y$. The earlier integrals can thus be thought of as integrating over a single-layer point charge distribution ($K_1$ and $K_3$ of charge density $g(y)$, without and with screening, respectively) and a double-layer point dipole distribution ($K_2$ and $K_4$ of dipole density $u(y)$, without and with screening, respectively) on the surface of the molecule.

## dBEM formulation

The first equation for surface point $x \in \partial\Omega$ of this formulation can be obtained by combining the two boundary integral equations, Eqs. 7 and 8, in the nBEM formulation, taking into consideration the interface condition, Eq. 3. The second equation can be obtained by taking the normal derivative along the direction of the outward normal vector at $x$. For a surface point $x$ in a smooth neighborhood, these two equations can be written as (Juffer et al., 1991)

$$\frac{1}{2}\left(1+\frac{\epsilon_e}{\epsilon_i}\right)\cdot u(x)-\int_{\partial\Omega}K_1(x,y)\cdot u(y)\cdot d\sigma_y + \int_{\partial\Omega}K_2(x,y)\cdot g(y)\cdot d\sigma_y=\sum_{i=1}\frac{q_k}{4\pi\epsilon_i|x-x_k|} \tag{10}$$

$$\frac{1}{2}\left(1+\frac{\epsilon_i}{\epsilon_e}\right)\cdot g(x)-\int_{\partial\Omega}K_3(x,y)\cdot u(y)\cdot d\sigma_y + \int_{\partial\Omega}K_4(x,y)\cdot g(y)\cdot d\sigma_y=\sum_{i=1}\frac{q_k}{4\pi\epsilon_i}\cdot\frac{\partial}{\partial n_x}\left(\frac{1}{|x-y|}\right) \tag{11}$$

where the kernels are now

$$K_1(x,y)=\frac{1}{4\pi}\cdot\frac{\epsilon_e}{\epsilon_i}\cdot\frac{\partial}{\partial n_y}\left(\frac{e^{-\kappa|x-y|}}{|x-y|}\right)-\frac{1}{4\pi}\cdot\frac{\partial}{\partial n_y}\left(\frac{1}{|x-y|}\right)$$
$$K_2(x,y)=\frac{1}{4\pi}\cdot\left(\frac{1}{|x-y|}-\frac{e^{-\kappa|x-y|}}{|x-y|}\right)$$
$$K_3(x,y)=\frac{1}{4\pi}\cdot\frac{\partial^2}{\partial n_x\partial n_y}\cdot\frac{e^{-\kappa|x-y|}}{|x-y|}-\frac{1}{4\pi}\cdot\frac{\partial^2}{\partial n_x\partial n_y}\frac{1}{|x-y|}$$
$$K_4(x,y)=\frac{1}{4\pi}\cdot\frac{\partial}{\partial n_x}\left(\frac{1}{|x-y|}\right)-\frac{1}{4\pi}\cdot\frac{\epsilon_i}{\epsilon_e}\cdot\frac{\partial}{\partial n_x}\left(\frac{e^{-\kappa|x-y|}}{|x-y|}\right) \tag{12}$$

Using these kernels, the interior and exterior potentials are

$$u^i(x)=\int_{\partial\Omega}K_1(x,y)\cdot u(y)\cdot d\sigma_y+\int_{\partial\Omega}K_2(x,y)\cdot g(y)\cdot d\sigma_y + \sum_{k=1}^{n}\frac{q_k}{4\pi\epsilon_i|x-x_k|},\quad x\in \text{int}\,\Omega,\quad y\in\partial\Omega \tag{13}$$

$$u^e(x)=\frac{\epsilon_i}{\epsilon_e}\int_{\partial\Omega}K_1(x,y)\cdot u(y)\cdot d\sigma_y + \frac{\epsilon_i}{\epsilon_e}\int_{\partial\Omega}K_2(x,y)\cdot g(y)\cdot d\sigma_y+\sum_{k=1}^{n}\frac{q_k}{4\pi\epsilon_e|x-x_k|},\quad x\in\mathbb{R}^3-\Omega,\quad y\in\partial\Omega \tag{14}$$

The regularity assumptions and the limiting process are argued in Juffer et al. (1991).

## Numerical method to solve the boundary integral equations

For numerical solution, we partition the surface of the molecule $\partial\Omega$ into a set of disjoint planar triangles $\Gamma_i$, so $\partial\Omega = \cup\Gamma_i$. We then approximate the unknowns $u(x)$ and $g(x)$ over a triangular element $\Gamma_i$ by linear interpolation of the nodal values of $u$ and $g$ of this triangle, using linear basis (shape) functions and barycentric coordinates. The nodal values of $u$ and $g$ are then the unknowns we seek. The integrals over the whole surface become the summation of elemental integration, which are carried out by numerical quadrature. Seeking the solutions to the nodal values of $u$ and $g$, we obtain $2M$ linear equations for a molecular mesh consisting of $M$ vertices. Conjugate gradient-based iterative solvers (GMRES and BICGSTAB) are then employed to solve these equations. Details of various numerical set-ups of BEM can be found in Banerjee and Walker (1981).

## ACCURATE REPRESENTATION OF THE MOLECULAR SHAPE

Under the continuum approach, different forms of the partial differential equations (PDEs) have been applied to model the molecular electrostatics: the Poisson equation (Warwicker and Watson, 1982; Zauhar and Morgan, 1985; Bharadwaj et al., 1995), the linearized Poisson-Boltzmann equation (Klapper et al., 1986; Davis and McCammon, 1990; Juffer et al., 1991), and the nonlinear Poisson-Boltzmann equation (Holst and Saied, 1995), each applicable under specific physical conditions (such as net charge of the molecule, the ionic strength, etc.). Of equal importance to the nature of the elliptic differential equation is the boundary descriptor, i.e., the accurate representation of the shape of the molecule. An exact molecular shape description is

therefore crucial for an accurate solution for the molecular electrostatics problem by the continuum model.

### Molecular surface mesh generation with topological precision

An important development for geometric modeling of macromolecules is the application of Delaunay complexes and the related alpha shape theory of alpha complexes. Alpha shape theory provides a topologically precise method for analytical computation of the molecular shape. In this method, the weighted Delaunay triangulation of the atom centers of the molecule is first computed (Edelsbrunner and Shah, 1992). The Delaunay complex obtained consists of tetrahedra, triangles, and edges connecting the atom centers, and vertices representing the atom centers. The alpha complex is then obtained by sorting the elements by using a ball-growth model (Edelsbrunner and Mücke, 1994). In addition to the vertices, the alpha complex retains a subset of the Delaunay tetrahedra, triangles, and edges, each corresponding to an occurrence of overlapping of the atom balls. The molecule and the alpha complex correspond to each other at topological, combinatorial, and metric levels. Algorithms have been developed to compute analytical molecular shapes for molecules, including the calculation of analytical area/volume ratio of the solvent-accessible (SA) model and the molecular surface (MS) model (Liang et al., manuscript submitted for publication), identification and measurements of inaccessible cavities in molecules (Liang et al., manuscript submitted for publication), and quantitative computation of the molecular pockets and analytical construction of receptor-binding sites (Edelsbrunner et al., 1996).

In this work, we employ an alpha shape-based method to topologically triangulate the surface of the molecule (Akkiraju and Edelsbrunner, 1996). The high-quality mesh generated allows precise representation of the molecular shape and maintains a convenient data structure for easy access to geometric and topological information contained in the mesh. Details of the mesh generation can be found in Akkiraju and Edelsbrunner (1996).

### Analytical representation of curve-shaped panel

For boundary integral equation-based BEM methods, the representation of the surface $\partial\Omega$ based on the mesh of planar triangles is important: curved panels are necessary to accurately represent both the shape of the surface integration domain and to evaluate the kernels. All interior points of the planar triangles therefore need to be mapped onto the atomic spheric surfaces.

Instead of using a quadratic or cubic function of the local coordinates in a planar triangle to approximate the spherical surface (Zauhar and Morgan, 1990; Juffer et al., 1991), here we describe an analytically exact method to map a planar point to the spherical patch. We exploit the fact that in the solvent-accessible surface model, the surface of the molecule consists of pieces of surface patches with known analytical expressions. Our representation is piecewise $C\infty$ (differentiable to degree infinity in the interior of each patch) and therefore is faithful to the original geometric model of the molecule (Lee and Richards, 1971). This method builds on the fact that geometric information is readily available from the data structure of the alpha shape-generated mesh.

In the SA model, we first compute the vector $v \in \mathbb{R}^3$ from the center of the atom to the planar point $r \in \mathbb{R}^3$. Normalization of $v$ will give the unit vector normal $n(r') = v/\|v\|$ to the surface point $r' \in \mathbb{R}^3$ to be mapped, which is on the spherical surface. We obtain the spherical point $r'$ by

$$r' = r + f \cdot n(r')$$

where $f = (R - \|v\|)/\|v\|$, where $R$ is the radius of the atom (see Fig. 1). The Jacobian determinant of this transformation is $|J(r')| = 1/|k(r) \cdot n(r')|$, where $k$ is the normal vector of the planar triangle. Geometrically, it is the ratio of the area of an infinitesimally small surface piece and the area of its projection on the planar triangle.

## NUMERICAL QUADRATURE

The formulae for the kernels of the boundary integral equations (Eqs. 9 and 12) reveal a difficulty in their integrations: these integrands become singular when $y$ approaches $x$. The integral of these kernels all have interpretations: these kernels are either weakly singular, or have Cauchy principal values, or their finite parts in the Hadamard sense exist (Kutt, 1975; Kaya and Erdogan, 1987). For example, the formula for kernel $K_3(x, y)$ in Eq. 12 has two terms, each of which is hypersingular, but it has been shown that $K_3(x, y)$ as the difference of the two hypersingular terms is itself integrable and well behaved (Juffer et al., 1991).

In BEM, these singularities hamper the numerical integration when $x$ and $y$ are on the same element (singular case), or when they are very close (near-singular case). Any

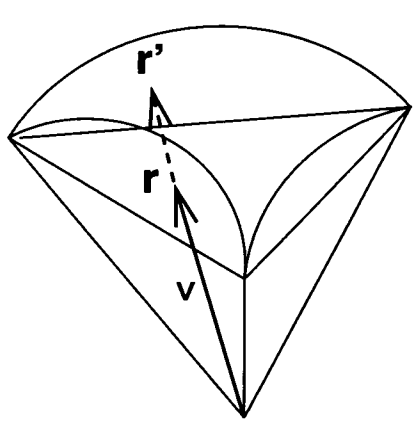


FIGURE 1 Mapping points on a planar triangle to the surface of the atom. The point $r$ on the planar triangle is mapped to the point $r'$ on the surface by extending $v$. $v$ is the vector starting from the center of the atom and ending at $r$.

quadrature rule of fixed weights (such as increasing the number of Gaussian quadrature points) is inadequate for the singular case, because these input-sensitive integrals are strongly influenced by the exact local shape of the element (Schwab and Wendland, 1992). For the near-singular case, although the integrals are regular, their numerical behavior is sensitive: the Gauss formula loses its asymptotic accuracy because the estimated error is influenced by the derivative of the kernels, which produce negative powers of the step size, canceling the asymptotic gain from using a higher order formula (Hackbusch and Sauter, 1994). In the molecular electrostatic problem, previous applications of BEM often use Gaussian quadrature for singular integrands, and the problem of near-singular integrands has been overlooked.

The accurate evaluation of the integration of the kernels, multiplied by the shape (basis) functions, is one of the key issues in the BEM, because the resulting singular diagonal elements of the matrix strongly affect the whole solution. Although analytical formulae are possible for planar triangle elements, integration over curved geometric elements is only plausible with numerical quadrature rules. In numerical analysis, the quadratures for singular integrands and near-singular integrands have been a very active research field in the past decade (Johnson and Scott, 1989; Guermond, 1992; Schwab and Wendland, 1992; Hackbusch and Sauter, 1994).

In our approach, we map all planar triangles $\Gamma_i$ to a standard simplex or a master triangle (0.0, 0.0; 0.0, 1.0; 1.0, 0.0) where the singular point is mapped to (0.0, 0.0). Numerical integration is then carried out over this standard triangle for all patches of the surface. The mapping from a planar triangle to a spherical triangular patch is as described earlier. Our method of numerical integration over the planar triangle is adapted from Guermond, (1992), where error analysis of several classes of kernels are available for curved elements.

## Singular integrand

Briefly, for the radial variable, we use a polar transformation to weaken the singularity. The new variable $\xi_1 \in [0, 1]$ is chosen such that

$$d\xi_1 = \frac{dr}{r(\phi)} \tag{15}$$

In the master triangle, we further express $r(\phi)$ as

$$r(\phi) = \frac{h}{\sin(\alpha + \phi)}$$

where $h$ is the height of the triangle from the side opposite the singular node, and $\alpha = \pi/4$ (see Fig. 2).

For the azimuth angle variable, there are still large variations in $r(\phi)$ when angles are near either of the two edges for which the singular point is the common endpoint. The situation is worse when the angle apexed by the singular point in the underlying $\Gamma_i$ is obtuse. Numerically this introduces undesirable instability. A further transformation for the azimuth angle variable is therefore necessary, such that the quadrature sampling points can be distributed unevenly. To take into account the large variation with the angle variable, the sampling points in the vicinity of the two edges should be finer than those between the edges. The measure adapted to this situation is $d\phi/\sin\phi$ rather than $d\phi$. Modified from Guermond (1992), we use the new variable $\xi_2 \in [-1, +1]$ for the azimuth angle variable, such that

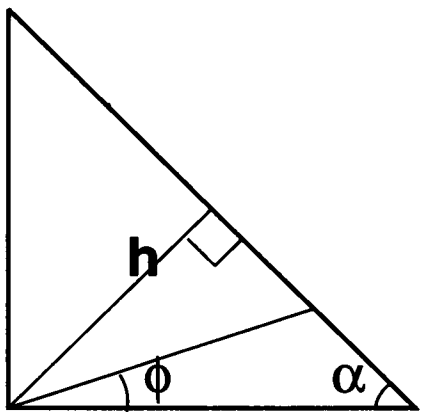


FIGURE 2 $h$ is the height of the triangle of the side opposite the singular node. $\alpha = \pi/4$ is the side angle. Sampling points along the radial line $r(\phi)$ are of angle $\phi$.

$$d\xi_2 = \frac{2 \cdot d\phi}{\Delta_k \cdot \sin(\phi + \alpha)} \tag{16}$$

where

$$\Delta_k := \int_{\alpha}^{\alpha+\pi/2} \frac{d\theta}{\sin\theta + \cos\theta} = 2\ln(1 + \sqrt{2}), \quad \alpha = \frac{\pi}{4}$$

From Eqs. 15 and 16, and the ranges of $\xi_1$ and $\xi_2$, we have the following transformation of the polar coordinates to the new variables $\xi_1$ and $\xi_2$ to be used in the Gaussian quadrature:

$$\xi_1 = r\frac{\sin(\alpha + \phi)}{h}$$

$$\xi_2 = \frac{1}{\Delta_k}\left(2\ln\left(\tan\frac{\phi + \alpha}{2}\right) - \ln\left(\tan\frac{\alpha}{2}\right) - \ln\left(\tan\frac{\pi/2 + \alpha}{2}\right)\right)$$

The transformations from the new variables $\xi_1$ and $\xi_2$ back to $r(\phi)$ and $\phi$ are

$$\phi = 2 \cdot \arctan(e^{\xi_2 \cdot \ln(1+\sqrt{2})}) - \frac{\pi}{4}$$

$$r = \frac{\xi_1 \cdot h}{\sin(\phi + \alpha)} = \frac{\xi_1}{\sqrt{2}\sin\left(\phi + \frac{\pi}{4}\right)},$$

Applying Gaussian quadrature to both $\xi_1$ and $\xi_2$ variables, we have the following quadrature rules:

$$\int_{\Gamma_i} K(x, y) \cdot u(y) d\sigma_y \approx \frac{\ln(1+\sqrt{2})}{\sqrt{2}} \sum_{n=1}^{N} \sum_{l=1}^{L} w_{2n} w_{1l} \cdot r_{ln} K(x, r_{ln}, \phi_n) \cdot u_i(r_{ln}, \phi_{ln}) \cdot J_i(r_{ln}, \phi_{ln}) \quad (17)$$

where $r_{ln} := r_l(\phi_n) = r_l(\xi_{2,n})$, $\phi_n = \phi(\xi_{2,n})$, and $N$, $L$ are the numbers of quadrature points of transformed variables $\xi_1$ and $\xi_2$.

### Nearly singular integrand

One remedy for the near-singular integrand is to expand the unknown functions with Taylor series into a known sharply changing function and an unknown smoothly varying function. This is roughly the "peak splitting" method used by Juffer et al. in evaluation of the potential (although it is not used to influence the matrix assembly) (Juffer et al., 1991). However, the Coulomb term dominates the Taylor expansion, because the majority of the atoms carry partial charges and cannot be treated as neutral. Hence the evaluation of the known function at one point in space will take $O(n)$ steps to sum over all charges. The surface integration (itself an $O(n^2)$ process, if all values of the function are known) will render the overall performance of the algorithm close to $O(n^3)$ time complexity for computing potential at one point in space. In the interest of practical time complexity, we do not follow this approach. Instead, we follow Guermond (1992): when $x$ is near the panel $\Gamma_i$, the standard simplex or the master triangle is subdivided into $P^2$ geometrically similar subsimplexes. We then apply Gaussian quadrature to each of these subsimplexes. In our implementation, we measure the distance $|x - y|$, and apply this scheme if the distance is smaller than the longest edge of the planar triangle. Details of error analysis of this rule can be found in Guermond (1992).

## RESULTS

### Conditioning of the boundary integral equations with dBEM

Conceptually, boundary integral equations lead to a dense, nonsymmetrical influence (coefficient) matrix for a system of linear equations to be solved numerically. In principle, the Poisson equation leads to a second kind Fredholm type integral equation, characterized by a well-conditioned compact integral operator. This significantly facilitates the solution of the resulting set of linear equations, and allows effective use of a class of iterative solvers (Barrett et al., 1994). In our cases, the nonintegral terms on the left-hand side of the boundary integral equations of dBEM distinguish these equations as the second kind of Fredholm-type integral equation. We use increasing numbers of triangular mesh elements to model a unit sphere, and we calculate the condition number of the resulting influence matrices. The condition number of a matrix $A$(cond($A$) = $\|A\| \cdot \|A^{-1}\|$) measures the sensitivity of the solution of a linear system to perturbation. It is a good indicator of the convergence behavior of many iterative solvers for linear equations, where floating point calculations are always accompanied by errors from finite arithmetic (Barrett et al., 1994). In all cases, the matrices of the second kind of integral equation resulting from dBEM have significantly lowered the condition number, as compared to the matrices where the nonintegral terms are left out.

However, the matrices from nBEM and dBEM have very different characteristics. This can be seen from the different forms of Eqs. 7, 8 and 10, 11, and from visualization of the coefficient matrices. Fig. 3 plots the coefficient matrices from both the nBEM and the dBEM formulations for a

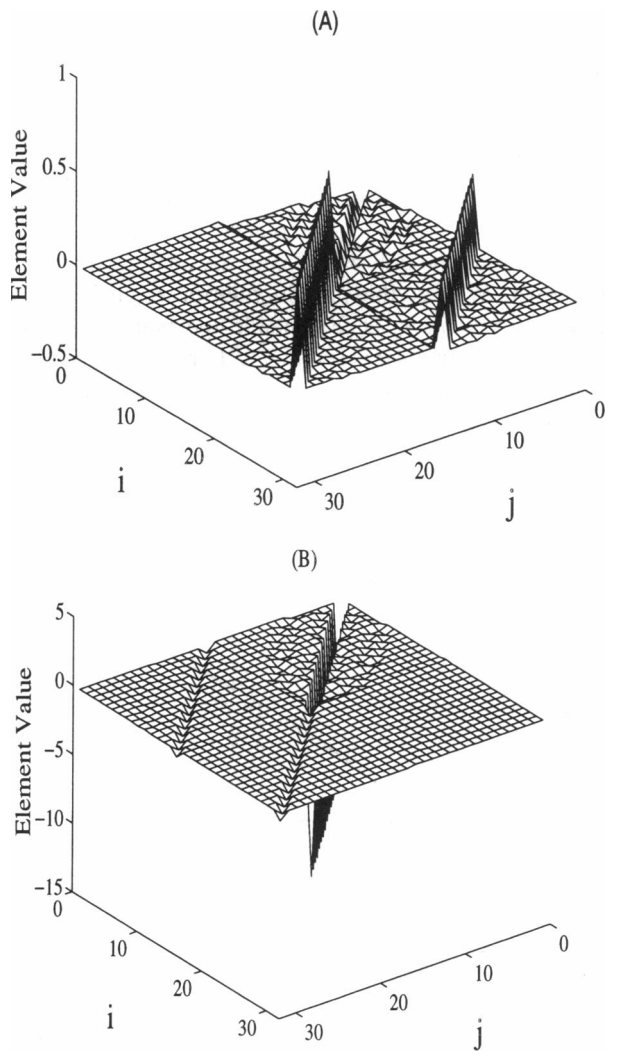


FIGURE 3 The final matrices obtained from 16-vertex triangulation of a unit sphere using both ($A$) nBEM and ($B$) dBEM. Matrices are formed using $\kappa$ = 3.0, $\epsilon_i$ = 1, and $\epsilon_e$ = 20.

16-vertex triangulation of a unit sphere. This suggests that nBEM and dBEM formulations may have different convergence behaviors for many numerical solvers. As an experiment, we use 16-, 32-, 64-, 128-, and 256-vertex triangulation of the unit sphere to test how the condition number scales with the size of the matrices from the two formulations. The sphere has the simplest geometry, and there is no effect due to complicated geometric considerations. As a result, such a test should reflect the characteristics of matrices due to the choice of formulation and exclude other factors. Fig. 4 shows that the condition numbers of the dBEM matrices (*empty circle*) are consistently small as the size of the matrix increases from 32 (for 16 vertex) to 512 (for 256 vertices). For nBEM (*filled circle*), the condition number deteriorates rapidly as the size of the matrix increases.

This has implications because rapid convergence of the linear equation solvers is an important issue in BEM, where meshes of large sizes are necessary to model molecules with complex geometry. There is no difference in terms of the storage required for dBEM and nBEM matrices. Therefore, we suggest that it is advantageous to use the dBEM formulation for a better conditioned influence matrix.

## Numerical tests

As a test case, we computed the electrostatic reaction potential of a unit point charge placed at various eccentric locations inside the unit ball, where the analytical solutions are known. We set the protein interior $\epsilon_i$ at 1, and the continuum solvent $\epsilon_e$ at 20 outside the ball. The inverse Debye-Buckel length $\kappa$ is set at 3/Å. For these calculations, dBEM formulation is used. An iterative solver (BICGSTAB) is used for solving the resulting linear equations

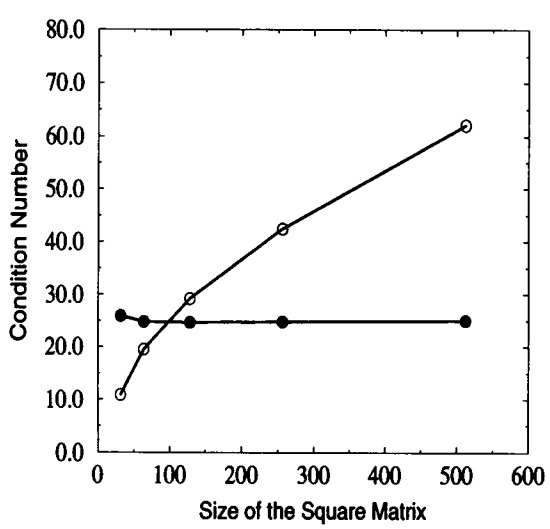


FIGURE 4 The condition numbers of the matrix formed by dBEM (●) are constantly small as the matrix size increases, whereas the condition number for nBEM matrices (○) deteriorates rapidly. Matrices are formed using $\kappa = 3.0$, $\epsilon_i = 1$, and $\epsilon_e = 20$.

(van der Vorst, 1992), with the convergence residue set at $1.0 \times 10^{-8}$. The results are listed in Table 1. The improvement of accuracy of the solution can be seen as the number of vertices used for triangular elements increases. The iteration numbers for the BICGSTAB solver indeed are small and show little increase as the number of vertices used to triangulate the sphere increased from 64 to 512. This agrees with our earlier assessment based on condition number calculations.

For comparison, we have also implemented the nBEM formulation for computing the reaction potential for a unit ball. The computed solutions have errors comparable to those of dBEM. However, the numbers of iterations carried out with BICGSTAB solver are very different, as seen in Table 2. Compared to the dBEM method, the iteration numbers are larger for all levels of discretization. The nBEM iteration numbers also increase as the discretization becomes finer, and this is in contrast to the dBEM method. These results demonstrate that dBEM can provide accurate solutions with a better conditioned influence matrix. This is reflected by the fact that in the examples studied, the number of iterations required to achieve comparable accuracy is invariant with mesh size.

Fig. 5 shows the electrostatic potentials computed through dBEM at the $y$-$z$ plane of $x = 8.0$ Å when an ammonia molecule ($NH_3$) is placed in an infinite solution, centered at the origin, with its N atom on the $z$ axis. $\epsilon_i$ and $\epsilon_e$ are set at 2.0 and 80.0, respectively. The temperature and the monovalent ionic strength are set at 298 K and 150.0 mM. The molecule is triangulated by 492 elements. Fig. 5 shows the potential surface on the $x$-$y$ plane. In $NH_3$, the N atom has a negative partial charge and H atoms have positive partial charges. The $y$-$z$ plane has an asymmetrical pattern in which the high $z$ part is negative and the low $z$ part is positive, consistent with the locations of negative N ($z = 0.110$ Å) and positive H ($z = -0.256$ Å) atoms. Fig. 6 shows the potentials computed through dBEM at the $x$-$y$ plane of $z = 8.0$ Å. The patterns of the potentials are rather symmetrical, consistent with the geometric symmetry of the molecule.

As a preliminary study of protein electrostatics, we compute the potentials near a crambin molecule on the $x$-$z$ planes at fixed $y = -10$ Å, i.e., beneath the molecule, and at $y = 26$ Å, i.e., above the molecule. The crambin molecule placed in an infinite medium has all of its atom centers located in the following coordinate ranges: $x \in [-3.51$Å, 25.02Å], $y \in [-0.967$Å, 20.867Å], $z \in [-7.383$Å, 19.238Å] and is centered at ($-1.407$ Å, $-0.684$ Å, $-3.911$ Å). The surface of the molecule is tiled with a mesh consisting of 1962 triangle elements to correctly preserve all topological features. Using a precomputed Delaunay complex and the alpha shape of crambin, the mesh is generated in 4.91 cpu s on a 195-MHz R10000 SGI machine. The Delaunay complex and the alpha shape of crambin are computed in 4.1 and 7.4 cpu s, respectively, on the same machine. Fig. 7 shows the potentials for the $y = -10$ Å plane, and Fig. 8 shows the potentials for the $y = 26$ Å

**TABLE 1 Computed reaction potential due to a unit charge placed inside a unit ball at various eccentric locations**

| $d$ | Exact | Iteration | Error | Iteration | Error | Iteration | Error | Iteration | Error | Iteration | Error |
|---|---|---|---|---|---|---|---|---|---|---|---|
| No. of | vertices | 16 | 16 | 64 | 64 | 128 | 128 | 256 | 256 | 512 | 512 |
| 0.0 | −3.77184 | 5 | 4.29 | 7 | 1.28 | 8 | 0.67 | 8 | 0.35 | 6 | 0.18 |
| 0.1 | −3.80928 | 9 | 4.43 | 10 | 1.31 | 10 | 0.68 | 11 | 0.36 | 10 | 0.18 |
| 0.2 | −3.92544 | 9 | 4.87 | 11 | 1.39 | 12 | 0.72 | 12 | 0.37 | 10 | 0.19 |
| 0.3 | −4.13616 | 10 | 5.78 | 12 | 1.55 | 13 | 0.80 | 13 | 0.41 | 11 | 0.21 |
| 0.4 | −4.47250 | 11 | 7.62 | 13 | 1.84 | 14 | 0.93 | 16 | 0.48 | 13 | 0.25 |
| 0.5 | −4.99440 | 14 | 11.38 | 16 | 2.35 | 17 | 1.16 | 17 | 0.58 | 16 | 0.30 |
| 0.6 | −5.82816 | 13 | 18.74 | 15 | 3.38 | 15 | 1.66 | 16 | 0.80 | 16 | 0.42 |
| 0.7 | −7.26768 | 13 | 31.51 | 15 | 5.79 | 17 | 2.92 | 15 | 1.33 | 17 | 0.73 |
| 0.75 | −8.43504 | 14 | 40.21 | 15 | 8.26 | 17 | 4.41 | 16 | 1.92 | 18 | 1.06 |
| 0.80 | −10.19376 | 13 | 50.34 | 16 | 12.61 | 16 | 7.45 | 19 | 3.11 | 21 | 1.66 |
| 0.85 | −13.12656 | 14 | 61.65 | 19 | 20.55 | 18 | 13.82 | 21 | 6.00 | 22 | 2.88 |
| 0.90 | −18.97824 | 13 | 73.84 | 20 | 35.07 | 20 | 27.20 | 22 | 14.00 | 22 | 5.69 |

The potential is in units of $e/(\epsilon_0 \times \text{Å})$, where $e$ is the unit electron charge, and $\epsilon_0$ is the dielectric constant of vacuum. $d$ in the table is the distance of the charge from the center of the ball. The errors of the numerical results as a percentage compared to analytical solutions are listed along with the iteration number of the BICGSTAB solver (van der Vorst, 1992) with the convergence residue set at $1.0 \times 10^{-8}$. The inverse Debye-Huckel length $\kappa$ is set at 3/Å. A $7 \times 7$ Gauss quadrature rule is used for the nonsingular integrand, a $10(\phi) \times 5(r)$ quadrature rule as described in the paper is used for the singular integrand. For the intermediate integrand, level 3 subdivision and the $7 \times 7$ quadrature rule are used. Linear functions are used as the basis functions.

plane. The relative orientations of crambin are also shown (not to scale).

## DISCUSSION

BEM differs from FDM in that it makes it possible to maintain an accurate (implicit) global solution using an exact representation of the shape of the molecule (Zauhar and Varnek, 1996). FDM relies on techniques such as "focusing" to obtain accurate local solutions. The alpha shape-based mesh generation allows a very accurate description of the molecular shape for the BEM calculation, in which no erroneous triangles will be added to connect across clefts and surface invaginations. It also faithfully represents the topological features of the molecule, such as all of the inaccessible cavities inside the molecule.

The kernel singularities of the boundary integral equations are one of the distinctive characteristics of the BEM method. The strength of the singularities strongly affects the condition number of the resulting coefficient matrix. Several methods have been described to solve the singularity problem. Yoon and Lenhoff (1990) analytically integrated the kernels for the nBEM formulation. However, in general the analytical evaluation of singular kernels (Kaya and Erdogan, 1987) can be prohibitive in terms of the algebraic derivation: it is only plausible when planar boundary elements are used (as in Yoon and Lenhoff, 1990). It is not clear what errors are introduced by using planar as opposed

**TABLE 2 Iteration numbers of the BiCGSTAB solver, using nBEM formulation for computing reaction potential due to a unit charge placed inside a unit ball**

| $d$ | Iteration number | | | | | |
|---|---|---|---|---|---|---|
| No. of vertices | 16 | 32 | 64 | 128 | 256 | 512 |
| 0.0 | 5 | 15 | 18 | 22 | 24 | 25 |
| 0.1 | 10 | 17 | 19 | 22 | 32 | 33 |
| 0.2 | 10 | 21 | 19 | 27 | 31 | 37 |
| 0.3 | 11 | 21 | 23 | 26 | 29 | 36 |
| 0.4 | 12 | 20 | 21 | 31 | 41 | 37 |
| 0.5 | 14 | 24 | 27 | 36 | 37 | 50 |
| 0.6 | 14 | 23 | 30 | 46 | 52 | 43 |
| 0.7 | 15 | 25 | 40 | 57 | 62 | 45 |
| 0.75 | 17 | 36 | 36 | 50 | 58 | 58 |
| 0.80 | 16 | 34 | 41 | 47 | 57 | 56 |
| 0.85 | 19 | 34 | 42 | 47 | 62 | 62 |
| 0.90 | 21 | 40 | 39 | 57 | 75 | 65 |

All parameters are the same as described in Table 1.

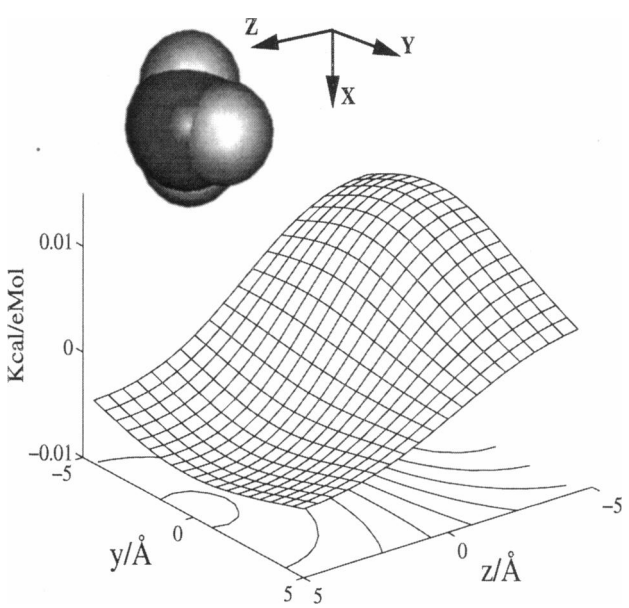


FIGURE 5 The electrostatic potentials at the $y$-$z$ plane of $x$ = 8.0 Å computed through dBEM. The potential surface shown is 8.0 Å below the center of the molecule along the positive $x$ direction (the *inset* shows the orientation of the ammonia molecule). The ammonium molecule ($\epsilon_i$ = 2.0) centering at the origin is placed in an infinite monovalent ionic solution (150.0 mM, 298 K, $\epsilon_e$ = 80.0). It is triangulated with 492 triangles.

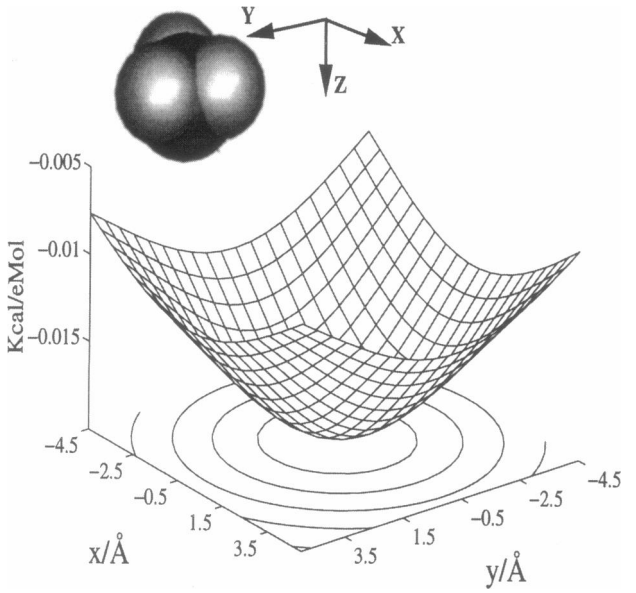


FIGURE 6 The electrostatic potentials at the $x$-$y$ plane of $z = 8.0$ Å for the same ammonium system computed through dBEM. The potential surface shown is 8.0 Å below the center of the molecule along the positive $z$ direction (the *inset* shows the orientation of the ammonia molecule).

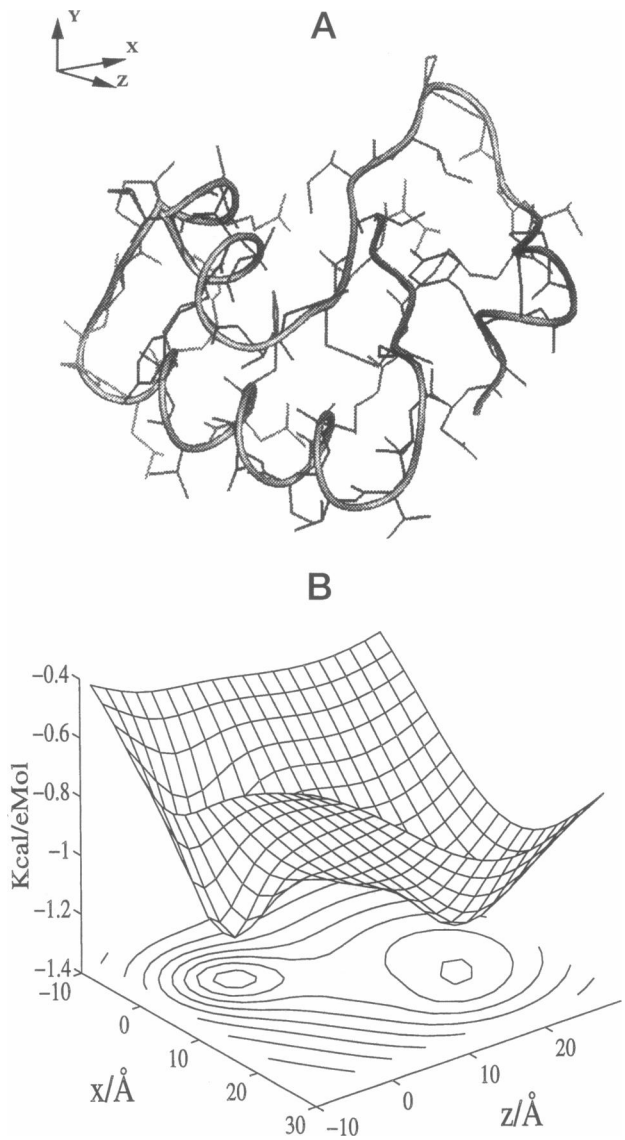


FIGURE 7 The electrostatic potentials computed through dBEM on a $x$-$z$ plane of $y = -10.0$ Å near a crambin molecule placed in an infinite medium. (A): the orientation of the crambin molecule (not to scale). (B): the potential surface at $y = -10.0$ Å.

to curved boundary elements. However, the number of elements required for a precise description is lower in curved-element representations.

When ion effects from the continuum model are ignored, the Poisson equation is used to model the molecular electrostatics. For such cases, Purisima and Nilar used a "row-sum elimination" method to obtain the singular integration term (Pursima and Nilar, 1995). It is based on the fact that the solid angle subtended by a part of a smooth surface is one-half of the full solid angle ($4\pi$). This method cannot be extended for two reasons. First, for the linearized Poisson-Boltzmann equation where ion effects are included, no simple geometric formulae are known for kernels of the type in Eq. 9 ($K_3$, $K_4$), and 12 ($K_1$ to $K_4$) to be used for subtraction. Second, when the potential inside each element is not treated as a constant, the solid angle formula cannot be applied, because the basis functions that are used to interpolate between nodal values cannot be separated out from the integrand. On the other hand, Guermond showed that nonconstant interpolation of the potential within each element is necessary to achieve an accurate solution, if the use of a modest number of mesh elements is desired (Guermond, 1994).

The conditioning of the boundary element equations is an important and complicated issue. We have shown that the dBEM formulation has an advantage over nBEM formulation: it results in a better conditioned influence matrix, and this formulation alone maintains a matrix with a good condition number, even when the problem scales up. The overall conditioning of the boundary element equations is necessarily a complicated issue, and depends on other factors, including the shape of the molecule, the discretization of the surface of the molecule, the choice of the shape (basis) functions for approximating potentials within each element, and the approximation of the surface. Together with the numerical integration scheme, these factors also affect the accuracy of the solution. Further investigations in these directions will provide valuable information.

Multipole expansions have recently been used to rapidly compute, either explicitly or implicitly, the influence matrix for the Poisson equation (Bharadwaj et al., 1995; Zauhar and Varnek, 1996). However, such efforts are currently confined to the Poisson equation where modeling of the ion effects are not possible. The reason behind is that the multipole expansions of the Green's function (and its derivative) for the linearized Poisson-Boltzmann equation (e.g., $K_3$ and $K_4$ in Eq. 9) have not been worked out.

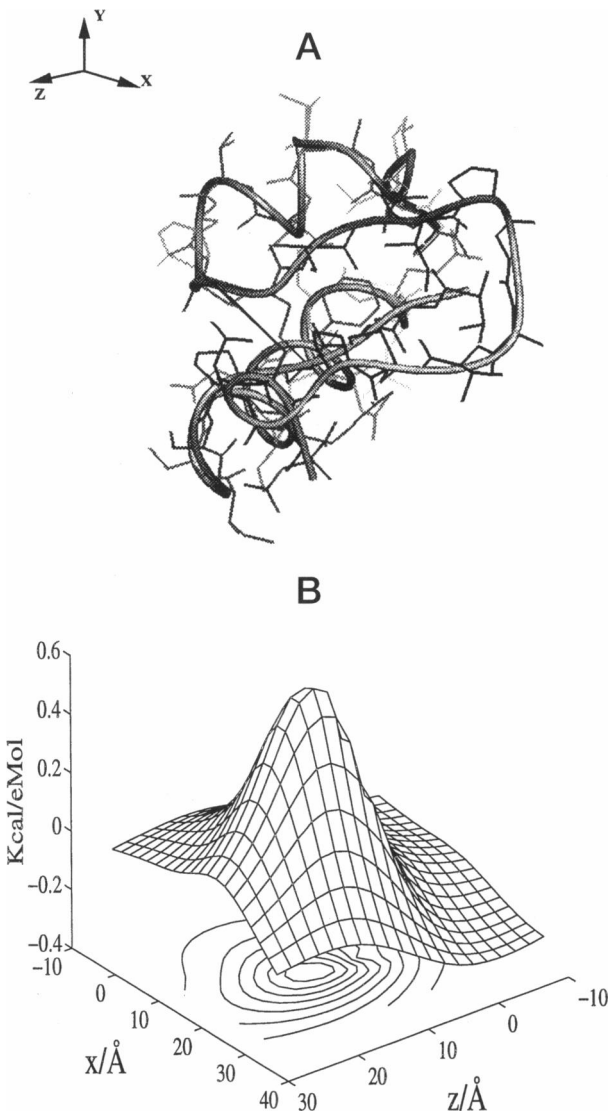


FIGURE 8 The electrostatic potentials computed through dBEM on an $x$-$z$ plane of $y$ = 26.0 Å near a crambin molecule placed in an infinite medium. (*A*) Orientation of the crambin molecule (not to scale). (*B*) Potential surface at $y$ = 26.0 Å.

Nevertheless, future fast methods should also significantly benefit from a stable and better conditioned influence matrix obtainable from the dBEM formulation. This is particularly relevant if the state-of-the-art nonstationary conjugate gradient-based iterative solvers (e.g., GMRES, BICG-STAB, etc.) are used rather than the stationary iterative solvers such as Gauss-Seidel or the successive overrelaxation (SOR) methods.

To check the integrity of the mesh, Bharadwaj et al. (1995) use the following Euler relationship for refining mesh on a sphere:

$$f = 2v - 4$$

where $f$ is the number of triangles and $v$ is the number of vertices. The Euler characteristics relationship for an arbitrary closed surface in $\mathbb{R}^3$ is

$$\chi = v - e + f = 2 - 2g$$

where $\chi$ is the Euler characteristics number, $e$ is the number of edges, and $g$ is the number of genus of this closed surface. Also note that $2e = 3f$.

When the system of the molecule(s) computed has several disconnected components and/or inaccessible interior voids, the number of closed surfaces triangulated must be equal to the number of components plus the number of voids. The relationship $\chi = 2 - 2g$ still holds for each closed surface. For a general relationship in this situation, we introduce the Betti numbers. The 0 Betti number $\beta_0$ is the number of components; the 1 Betti number $\beta_1$ is the sum of genuses of the whole surface; the 2 Betti number $\beta_2$ is the number of voids. The general relationship is now

$$f = 2v - 4(\beta_0 - \beta_1 + \beta_2)$$

This relationship must hold for a correctly triangulated mesh. See Akkiraju and Edelsbrunner (1996) for more details.

To summarize our BEM work, because shape description is important for the continuum approach to the molecular electrostatics problem, we apply an alpha shape-based method to generate a topologically precise and analytically accurate surface mesh for molecules. We also describe the shape of the molecule analytically within each element, using a piecewise analytical function to represent the shape of the surface used in BEM. Contrary to the widely used nBEM formulation (Zauhar and Morgan, 1990; Yoon and Lenhoff, 1990; Zhou, 1993b), we show that the dBEM boundary integral equations provide superior numerical stability and should be used when speedy convergence in the solution of the linear equations is desired. Singular and near-singular kernel integrands can introduce large errors into the solution in BEM and must be treated carefully. We have described an effective method of variable transformation to be used for numerical quadratures.

## APPENDIX A: ALPHA SHAPE METHOD FOR MESH GENERATION

For molecular mesh generation, we apply a surface triangulation method using the alpha shape method (Akkiraju and Edelsbrunner, 1996). Briefly, a molecule is modeled combinatorically by an associated geometric construct, the dual complex, or the alpha complex at $\alpha = 0$. The concepts behind this method are the weighted Voronoi diagram, the weighted Delaunay complex, and the theory of alpha shapes.

The Voronoi diagram of the atom balls divides the space into Voronoi regions, one per atom. A Voronoi region is generated by an atom, and consists of the part of space "closest" to this atom. When the different radii of atoms are taken into consideration, we have the weighted Voronoi diagram. Adjacent Voronoi regions are separated by the radical plane of their atom balls. The Voronoi regions are always convex and are either disjoint or overlap along common boundary pieces. The Delaunay complex is a geometric construct that can be derived from the Voronoi diagram by the following direct translation. The center of an atom ball with a Voronoi region becomes a vertex in the Delaunay complex. If two Voronoi regions share a common facet, then the edge connecting the centers of the two

corresponding atom balls is in the complex. If three Voronoi regions share a common edge, then the triangle spanned by the three ball centers is in the complex. Finally, if four Voronoi regions share a common point, then the tetrahedron spanned by the four ball centers is in the complex. We have thus accounted for all possible intersection patterns among Voronoi regions, because in three-dimensional space there can be no more than four Voronoi regions that meet at one point. The vertexes, edges, triangles, and tetrahedra are the four basic types of elements, called *simplices*.

The dual complex (or the alpha complex at $\alpha = 0$) is a subset of the Delaunay complex, and consists of the four different types of simplices described above. The vertices are the centers of the atom balls. We add an edge connecting two atom centers to the dual complex if their two convex cells overlap along a common face. Similarly, we add a triangle spanned by three centers if their convex cells share a common edge. Finally, we add a tetrahedron spanned by four centers if their convex cells share a common point.

We refer to Edelsbrunner and Mücke (1994) and references within for a complete and rigorous treatment of weighted Voronoi diagrams, weighted Delaunay complexes, and the dual complex. An intuitive description can be found in Liang et al. (manuscript submitted for publication). Most importantly, the dual complex faithfully represents geometrical and topological features of the surface of the molecule. For example, the circle where the surfaces of two overlapping atoms meet can be computed explicitly by following the edge in the dual complex. The corner point where the surfaces of three atoms meet can be computed explicitly from the triangles in the dual complex. Circles and corners topologically define the boundaries of the surface patches of the molecule. An algorithm has been developed that selects points on each patch and connects them to form a connected surface patch tiled with triangles, with each patch bounded by fractions of circles and corners obtainable from the dual complex. Details of this method are described by Akkiraju and Edelsbrunner (1996).

## APPENDIX B: NUMERICAL ASPECTS OF BOUNDARY ELEMENT METHODS

The integral equations are solved numerically by a boundary element method. The unknowns $u$ and $g$ are approximated in finite dimensional space by continous functions. In our case, they are approximated by unique linear combinations of $N$ basis functions, where $N$ is the number of vertices on the surface. The $k$th basis function is linear and looks like a pyramid: it equals 1 at the $k$th vertex and 0 at all other vertices. It has nonzero values only on elements containing vertex $k$.

For the integral equations, the overall integrals are decomposed into summations of integrals over elements. Each surface triangle element is first transformed into a standard simplex (master triangle), where the numerical quadratures are applied for integration. In our case, we let the approximating trial functions for $u$ and $g$ satisfy the integral equations exactly on the $N$ vertices. As a result, we obtain a set of $2N$ linear equations. For Eqs. 10 and 11, the system of linear equations can be written as

$$(\mathrm{I} - A) \cdot x = f$$

where $I$ is the identity matrix, and $x$ is the $2N$ vector for the $N$ values of $u$ and $g$ on the vertices. Elements in $A$ are local surface integrals involving kernels $K_1$ through $K_4$. $f$ is the $2N$ vector for the source terms on the right-hand side of the equations. This linear system is then solved, for example, by a nonstationary conjugate gradient-based iterative solver.

We are indebted to Prof. Herbert Edelsbrunner for the topological surface triangulation that makes our approach possible. We thank Prof. Faisal Saied for many insightful discussions and suggestions, N. Akkiraju for generating the molecular meshes, and J. Bordner for help in implementing the iterative solver. JL thanks Lu Wang for helpful discussions.

JL is supported by an National Science Foundation (NSF) CISE postdoctoral fellowship (grant ASC 94-04900). SS acknowledges support by the NSF (grants ASC 89-02829 and MCB 92-19619) and the NSF Meta Center Computer Allocation.

## REFERENCES

Akkiraju, N., and H. Edelsbrunner. 1996. Triangulating the surface of a molecule. *Discrete Appl. Math.* 71:5–22.

Allison, S. A., J. A. McCammon, and S. H. Northrup. 1986. Dynamics of macromolecular interactions. *In* Coulombic Interactions in Macromolecular Systems. A. Eisenberg and F. E. Bailey, editors. American Chemical Society, Washington, DC. 216–231.

Banerjee, P., and S. Walker. 1981. Boundary Element Methods in Engineering Science. McGraw-Hill, New York.

Barrett, R., M. Berry, T. F. Chan, J. Demmel, J. Donato, J. Dongarra, V. Eijkhout, R. Pozo, C. Romine, and der H. V. Vorst. 1994. Templates for the Solution of Linear Systems: Building Blocks for Iterative Methods, 2nd Ed. SIAM, Philadelphia, PA.

Bharadwaj, A., A. Windemuth, S. Sridharan, B. Honig, and A. Nicholls. 1995. The fast multipole boundary element method for molecular electrostatics: an optimal approach for large systems. *J. Comput. Chem.* 16:898–913.

Brebbia, C., J. Telles, and L. Wrobel. 1984. Boundary Element Techniques: Theory and Applications in Engineering. Springer-Verlag, Berlin.

Bruccoleri, R. 1993. Grid positioning independence and the reduction of self-energy in the solution of the Poisson-Boltzmann equation. *J. Comput. Chem.* 14:1417–1422.

Davis, M., and J. McCammon. 1990. Electrostatics in biomolecular structure and dynamics. *Chem. Rev.* 90:509–521.

Edelsbrunner, H., M. Facello, and J. Liang. 1996. On the definition and the construction of pockets in macromolecules. *In* Biocomputing: Proceedings of the 1996 Pacific Symposium. L. Hunter and T. Klein, editors. World Scientific, Singapore.

Edelsbrunner, H., and E. Mücke. 1994. Three-dimensional alpha shapes. *ACM Trans. Graphics.* 13:43–72.

Edelsbrunner, H., and N. Shah. 1992. Incremental topological flipping works for regular triangulations. *In* Proceedings of the 8th Annual Symposium on Computer Geometry. ACM Press, New York., 43–52.

Gilson, M., A. Rashin, R. Fine, and B. Honig. 1985. On the calculation of electrostatic interactions in proteins. *J. Mol. Biol.* 183:503–516.

Guermond, J.-L. 1992. Numerical quadratures for layer potentials over curved domains in $\mathbb{R}^3$. *SIAM J. Numer. Anal.* 29:1347–1369.

Guermond, J.-L. 1994. High order numerical quadratures for layer potentials over curved domains in $\mathbb{R}^3$. *Comput. Methods Appl. Mech. Eng.* 116:257–263.

Hackbusch, W., and S. Sauter. 1994. On numerical cubatures of nearly singular surface integral arising in BEM collocation. *Computing.* 52: 139–159.

Holst, M., and F. Saied. 1995. Numerical solution of the nonlinear Poisson-Boltzmann equation: developing more robust and efficient methods. *J. Comput. Chem.* 16:337–364.

Johnson, C., and L. Scott. 1989. An analysis of quadrature errors in second-kind boundary integral methods. *SIAM J. Numer. Anal.* 26: 1356–1382.

Juffer, A., E. Botta, van B. Keulen, van der A. Ploeg, and H. Berendsen. 1991. The electric potential of a macromolecule in a solvent: a fundamental approach. *J. Comput. Phys.* 97:144–171.

Kaya, A., and F. Erdogan. 1987. On the solution of integral equations with strongly singular kernels. *Q. Appl. Math.* 45:105–122.

Klapper, I., R. Hangstrom, R. Fine, K. Sharp, and B. Honig. 1986. Focusing of electric fields in the active site of Cu-Zn superoxid dismutase: effects of ionic strength and amino acid modifications. *Proteins Struct. Funct. Genet.* 1:47–59.

Kutt, H. 1975. The numerical evaluation of principal value integrals by finite-part integration. *Numer. Math.* 24:205–210.

Lee, B., and F. M. Richards. 1971. The interpretation of protein structures: estimation of static accessibility. *J. Mol. Biol.* 55:379–400.

Madura, J., M. Davis, M. Gison, R. Wade, B. Luty, and J. McCammon. 1994. Biological applications of electrostatic calculations and Brownian dynamics simulations. *In* Reviews in Computational Chemistry, Vol. 5. K. Lipkowitz and D. Boyd, editors. VCH Publishers, New York. 229–267.

Pursima, E., and S. Nilar. 1995. A simple yet accurate boundary element method for continuum dielectric calculation. *J. Comput. Chem.* 16: 681–689.

Rashin, A., M. Iofin, and B. Honig. 1986. Internal cavities and buried wtares in globular proteins. *Biochemistry.* 25:3619–3625.

Schwab, C., and W. Wendland. 1992. On numerical cubatures of singular surface integrals in boundary element methods. *Numer. Math.* 62: 343–369.

Sharp, K., and B. Honig. 1990. Electrostatic interactions in macromolecules: theory and application. *Annu. Rev. Biophys. Biophys. Chem.* 19:301–332.

van der Vorst, H. 1992. Bi-CGSTAB: a fast and smoothly converging variant of Bi-CG for the solution of nonsymmetric linear systems. *SIAM J. Sci. Stat. Comput.* 13:631–644.

Warwicker, J., and H. Watson. 1982. Calculation of the electric potential in the active site cleft due to a $\alpha$-helix dipoles. *J. Mol. Biol.* 157:671–679.

Yoon, B., and A. Lenhoff. 1990. A boundary element method for molecular electrostatics with electrolyte effects. *J. Comput. Chem.* 11: 1080–1086.

Zauhar, R., and R. Morgan. 1985. A new method for computing the macromolecular electric potential. *J. Mol. Biol.* 186:815–820.

Zauhar, R., and R. Morgan. 1988. The rigorous computation of the molecular electric potential. *J. Comput. Chem.* 9:171–187.

Zauhar, R., and R. Morgan. 1990. Computing the electric potential of biomolecules: application of a new method of molecular surface triangulation. *J. Comput. Chem.* 11:603–622.

Zauhar, R., and A. Varnek. 1996. A fast and space-efficient boundary element method for computing electrostatic and hydration effects in large molecules. *J. Comput. Chem.* 17:864–877.

Zhou, H.-X. 1993a. Boundary element solution of macromolecular electrostatics: interaction energy between two proteins. *Biophys. J.* 65: 955–963.

Zhou, H.-X. 1993b. Brownian dynamics study of the influence of electrostatic interaction and diffusion on protein-protein association kinetics. *Biophys. J.* 64:1711–1726.